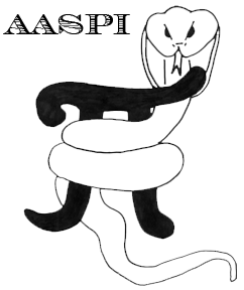

COMPENSATING FOR MIGRATION STRETCH – PROGRAM compensate_for_migration_stretch

Contents

Computation flow chart

The input to program **compensate_for_migration_stretch** consists of migrated seismic gathers and either an RMS or migration velocity model. The output is a volume of gathers that have been compensated for migration stretch. Optional output files include the residual gathers, the correction factor, and the wavelet dictionary used in the matching pursuit algorithm.

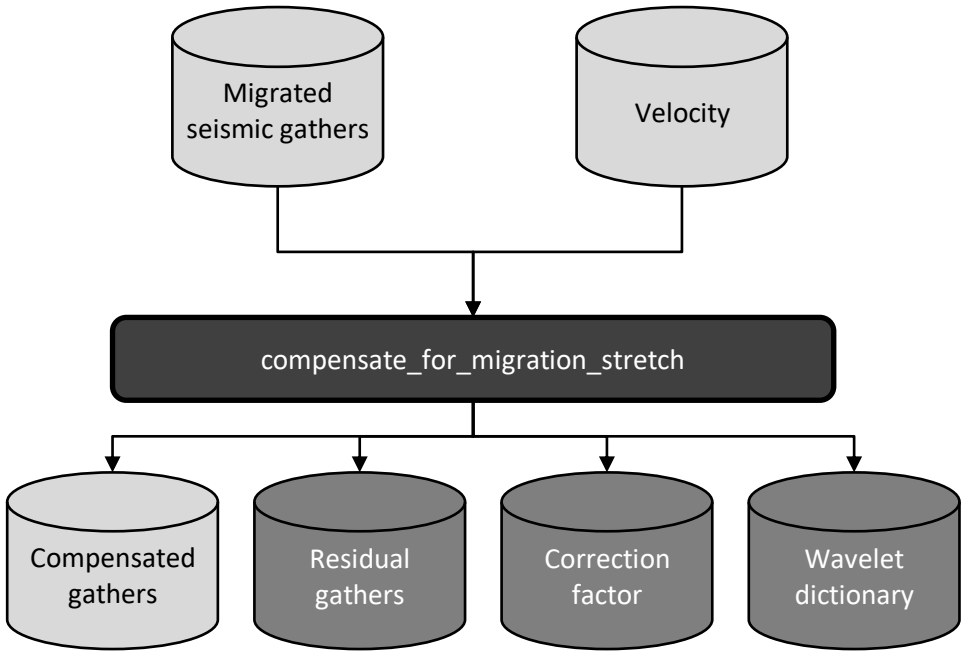

Figure 1.

Output file naming convention

Program **compensate_for_migration_stretch** will always generate the following output files:

Output file description	**File name syntax**
Compensated data gathers	d_compensated_*unique_project_name_suffix*.H
Program log information	d_compensate_for_migration_stretch_*unique_project_name_suffix*.log
Program error/completion information	d_compensate_for_migration_stretch _*unique_project_name_suffix*.err

The errors we anticipated will be written to the **.err* file and be displayed in a pop-up window upon program termination. These errors, much of the input information, a description of intermediate variables, and any software trace-back errors will be contained in the **.log* file. Depending on the parameters selected in the GUI, the following optional files may also be generated:

Output file description	**File name syntax**
Residual data not modeled by the matching pursuit algorithm	d_residual_*unique_project_name_suffix*.H
Stretch compensation factor	compensation_factor_*unique_project_name_suffix*.H
Wavelets used in matching pursuit	wavelets _*unique_project_name_suffix*.H

Invoking the compensate_for_migration_stretch GUI

The **compensate_for_migration_stretch** GUI is found on the **aaspi_util_prestack** GUI under the *Prestack Data Conditioning* tab:

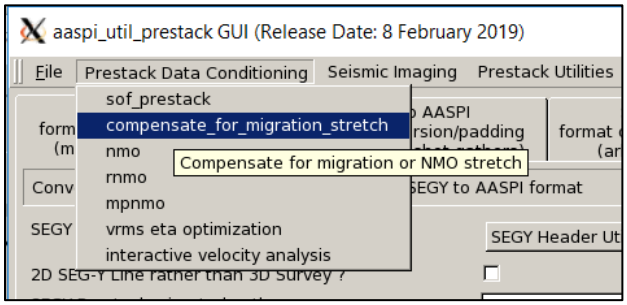

The GUI has the parameters associated with an NMO correction, but also those used in matching pursuit spectral decomposition algorithm **spec_cmp**:

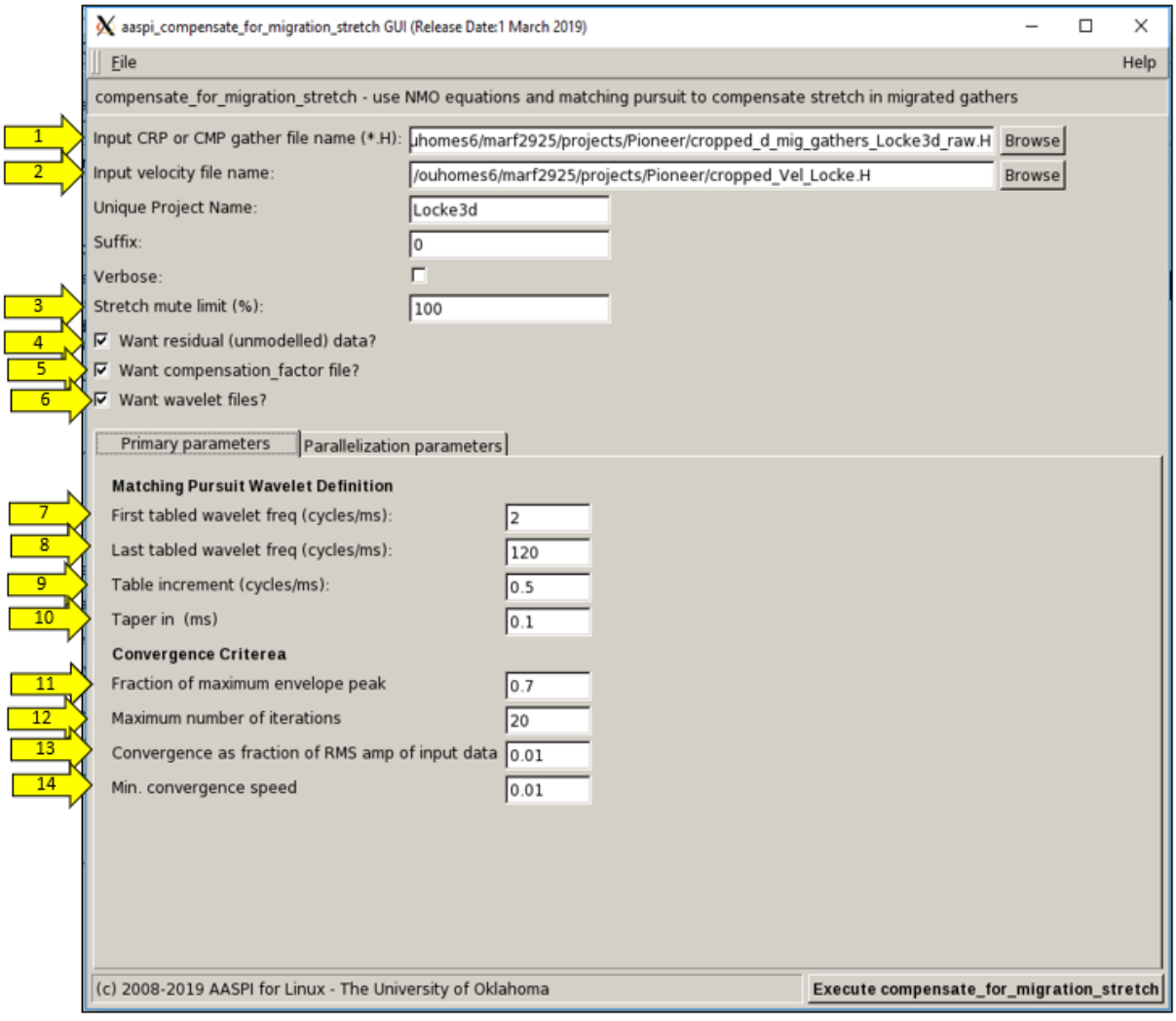

Simply (1) enter the name of the file containing the migrated (or previously NMO-corrected) gathers, and (2) the corresponding velocity file. Common stretch-mute corrections on uncompensated data range between 20 and 30%. This algorithm (3) compensates for significantly greater amounts of stretch mute where the default value of 100% will compress correspondingly stretched wavelets by a factor of 2.

The output stretch-compensated file will have a name of the form *d_compensated_unique_project_name_suffix.H* . To better evaluate the performance of the algorithm, you may wish to output several optional files, (4) the residual (unmodelled part of the gather), (5) the stretch correction (which will always be greater than or equal to 1, and (6) the wavelet library used in the decomposition. As shown in the algorithm flow chart below, the wavelet library is precomputed and does affect the run time. In general, the choice of wavelets (7)-(9) should span the useable frequencies in the seismic data. The edges of the data need to be (10) tapered. Options (11)-(14) define the convergence criteria, including a value β that ranges $0< \beta \leq 1$ defined in the algorithm flow chart. If β is close to zero, all envelope peaks will be used in the first iteration. If β=1, only the largest envelope peak will be used, resulting in a "greedy" matching pursuit algorithm and longer run times. Reasonable values of β should be greater than 0.5. The algorithm ends when the (12) the maximum number of iterations is reached, (13) convergence is achieved, or (14) convergences slows down to an unacceptable level. Further information on these parameters can be found in the documentation for program **spec_cmp**.

The NMO Correction and NMO-Stretch

If the vertical two-way travel time is given by T_0, then the travel time for the same flat reflector at source-receiver offset h for velocity v_{RMS} is given by

$$t(T_0, v_{RMS}, h) = \left\{ T_0^2 + \left[\frac{h}{v_{RMS}(T_0)} \right]^2 \right\}^{1/2}, \quad (1)$$

where each trace is defined by a fixed offset, h. The change in two-way travel time t, as a function of the zero-offset travel time T_0 is simply

$$\frac{\partial t}{\partial T_0} = T_0 \left\{ T_0^2 + \left[\frac{h}{v_{RMS}(T_0)} \right]^2 \right\}^{-1/2} < 1, \quad (2)$$

which always has a value less than 1. For this reason, an event after NMO at time T_0 is always stretched with respect to the original event at time t.

The Convolutional Model and Compensating for NMO- or Migration-Stretch

Let's assume the earth is composed of a suite of *J* reflections at time t_j and reflection coefficient r_j. Let's also assume that time-varying source wavelet can be represented by Morlet wavelets of the form $w(f_j, \phi_j)$. The seismic trace without the NMO correction is then

$$u(t) = \sum_{j=1}^{J} r_j \delta\left(t_j\right) w\left(f_j, \varphi_j\right). \tag{3}$$

After an NMO correction, these wavelets are stretched. Mapping T_{0j} to t_j using equation 1, we can compute a wavelet compression factor, *c*, from equation 2

$$c_j = \frac{1}{T_{0j}} \left\{ T_0^2 + \left[\frac{h}{v_{RMS}\left(T_0\right)} \right]^2 \right\}^{1/2} > 1, \tag{4}$$

which can then be used to scale the wavelets in equation 3 and generate the compensated trace

$$u_{comp}(T_0) = \sum_{j=1}^{J} r_j \delta\left(T_{0j}\right) w\left(c_j f_j, \varphi_j\right). \tag{5}$$

In this manner, compensation for migration stretch is a process that involves several simple steps:

Algorithm flow chart

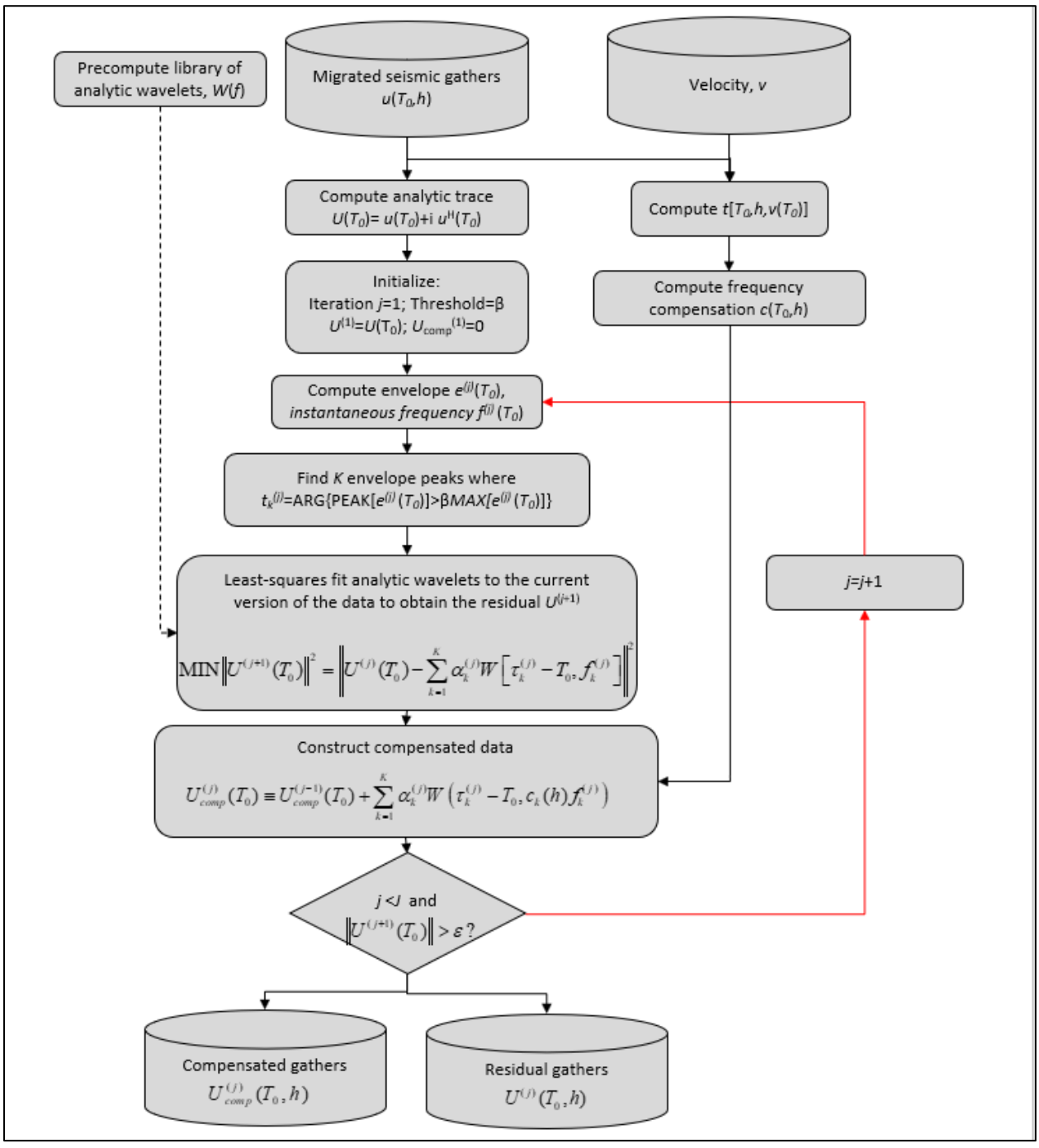

Figure 2.

An example of the wavelets used in the matching pursuit decomposition. The first panel shows the real and second the imaginary components of the wavelets.

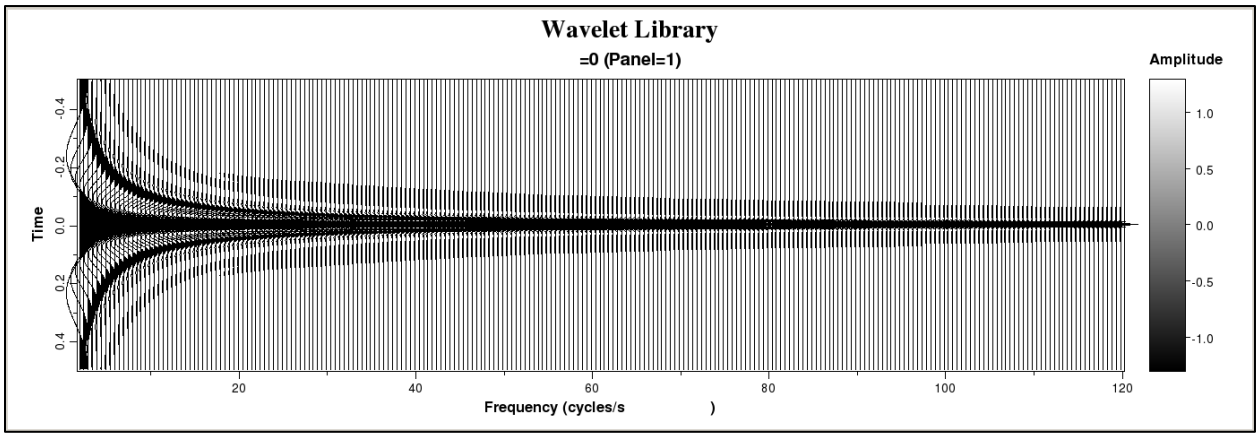

Figure 3.

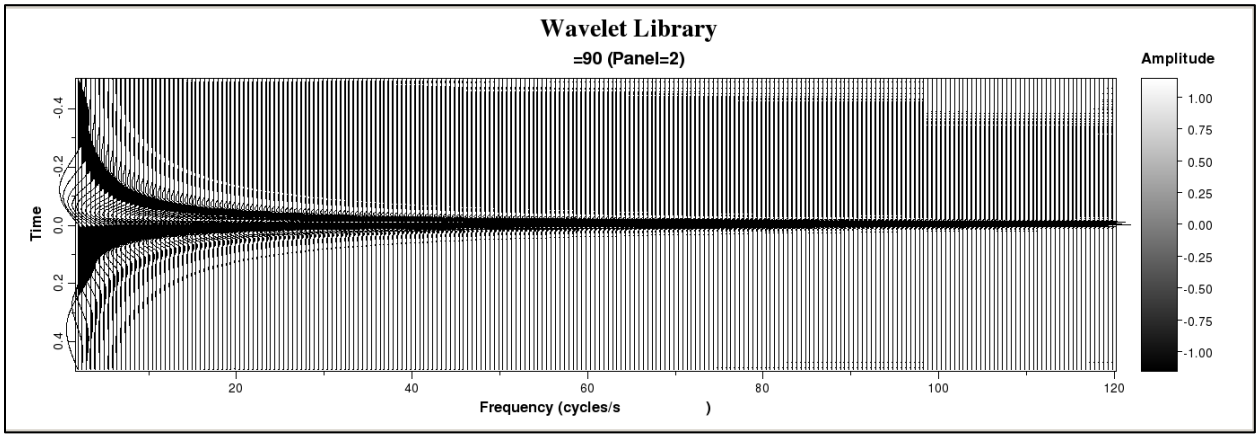

Figure 4.

Theory: Implementation of the matching pursuit algorithm

Matching pursuit (e.g. Castagna and Sun, 2006; Liu and Marfurt, 2007) works in a manner similar to high resolution Radon transforms, where the spectra of the strongest events are estimated and subtracted from the trace first, followed by iterative estimation and subtraction of successively weaker events. Since their originally introduction, more general basis pursuit algorithms that use a suite of nonorthogonal basis functions as well as L1 norms applied to the data misfit and L1 constraints to minimize the number of components have been found to be quite effective in improving the resolution of seismic data (e.g. Puryear and Castagna, 2011). In this appendix, we provide an updated description of the relatively simple matching pursuit algorithm used by Liu and Marfurt (2007).

We begin the analysis by assuming that each seismic time trace, *u(t)*, is band-limited and can be represented by a linear combination of *J* Morlet wavelets, *w*:

$$u(t) = \sum_{j=1}^{J} r_j \cdot w(t - t_j, f_j, \phi_j) + n(t),$$

(A-1)

where r_j, t_j, f_j and φ_j represent the reflection coefficient, center time, peak frequency, and phase of the j^{th} wavelet centered about time t_j, and $n(t)$ represents noise. In general, reflected events from thin beds, gradients in impedance, discontinuities in attenuation (1/Q), and inaccurately migrated events as well as dispersed events will have arbitrary phases even if the source wavelet is zero phase. For this reason, we construct our basis functions using a suite of complex Morlet wavelets (Figure A1). We calculate the center time t_j of each candidate wavelet using the peaks in the instantaneous envelope and the wavelet frequency, f_j, using the instantaneous frequency at the envelope peak.

The temporal behavior of a zero-phase Morlet wavelet is given by:

$$w(t, f_j) = \exp(-t^2 f_j^2 \cdot 2\ln 2) \cdot \cos(2\pi f_j t) \ ,$$

(A-2)

while its magnitude spectrum is given by:

$$\overline{w}(f, f_j) = \frac{\sqrt{\pi / \ln 2}}{f_j} \cdot \exp\left[-\frac{\pi^2 (f - f_j)^2}{2\ln 2 \cdot f_j^2} \right].$$

(A-3)

To efficiently solve for both the magnitude and phase of each wavelet, we use the Hilbert transform, and form both an analytic data trace, *U(t)*:

$$U(t) = u(t) + iu^H(t),$$

(A-4)

and a table of analytic complex wavelets:

$$W(t, f_j) = w(t, f_j) + iw^H(t, f_j) \ ,$$

(A-5)

where *w* are symmetric cosine wavelets given by equation A-2 and w^H are antisymmetric sine wavelets (Figure A-1).

Theory: Implementation of the matching pursuit algorithm (continued)

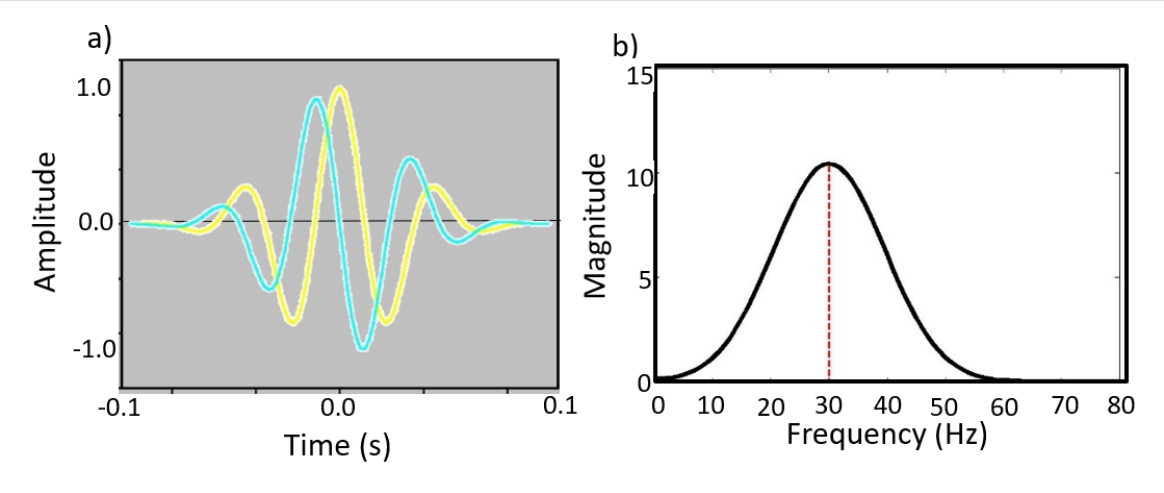

Figure A-1. (a) A complex 30 Hz Morlet wavelet consisting of a real part or 0° Morlet wavelet (yellow) and an imaginary part 90° Morlet wavelet (cyan). (b) The corresponding magnitude spectrum. (After Liu, 2006).

The first step in the matching pursuit algorithm is to precompute a finely sampled (wavelet dictionary that spans the bandwidth of the input data.

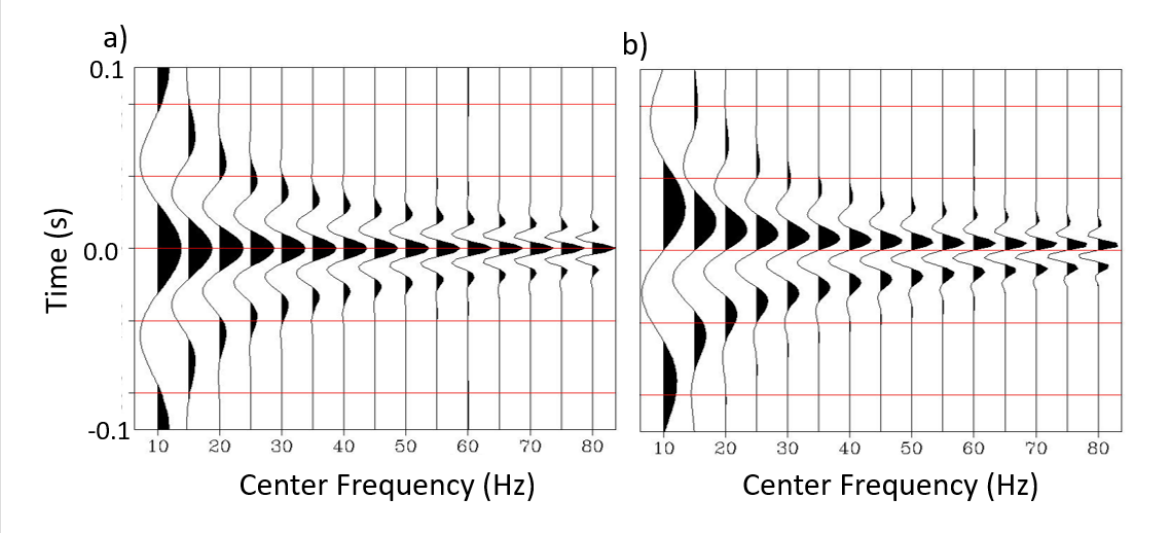

Figure A-2. Complex Morlet wavelets centered about t=0 s at Δf=5.0 Hz increments. In practice, the wavelets will be sampled at Δf=0.1 Hz rather than the 5.0 Hz increment shown here. (After Liu, 2006).

Theory: Implementation of the matching pursuit algorithm (continued)

The analytic analogue of equation A-1 then becomes:

$$U(t) = \sum_j A_j \cdot W_j(t - t_j, f_j) + N(\mathrm{t}), \tag{A-6}$$

where

$$e(t) = \|U(t)\|, \tag{A-7}$$

$$A_j = r_j e^{i\phi_j}, \tag{A-8}$$

and where $e(t)$ is the instantaneous envelope of the seismic trace, and r_j and φ_j represent the magnitude and phase of the complex wavelet W_j.

Our objective is to minimize the energy of the residual analytic trace, *R(t),* defined as the squared difference between the analytic seismic trace and the matched wavelets:

$$\|R(t)\|^2 = \left\| U(t) - \sum_j^J [A_j W_j(t - t_j, f_j)] \right\|^2 . \tag{A-9}$$

If we were to attempt to estimate all wavelet coefficients in one iteration, we would write equation A-9 in matrix form and simply solve the normal equations:

$$\mathbf{A} = [\mathbf{W^H W} + \varepsilon \mathbf{I}]^{-1} \mathbf{W^H U} \tag{A-10}$$

where **W**=[$W(t,f_1), W(t,f_2), \ldots, W(t,f_m)$] is a vector of wavelets centered of known frequency at each known envelope peak, $\mathbf{A} = (A_1, A_2, \ldots A_m)$ is a vector of unknown complex wavelet amplitudes, **I** is the identity matrix and ε is a small number which makes the solution stable. For seismic data, **A** will be a complex-symmetric banded matrix, with the bandwidth proportional to the number of samples used to define the lowest frequency wavelet used, and therefore amenable to efficient solution. Liu's (2006) Figure A-3 provides a graphical image of equation A-9 where the black and red curves represent the real part and imaginary parts of the complex trace and complex wavelets. .

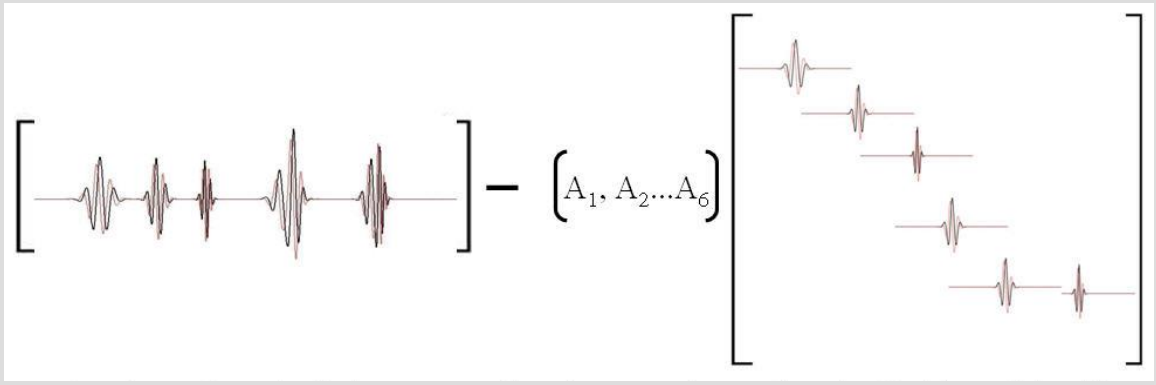

Figure A-3. (a) A complex seismic trace represented by (b) six complex amplitudes, and (c) six complex Morlet wavelets. The goal of equation A-9 is to compute the complex wavelet amplitudes A_j that when multiplied by W_j and summed, approximate the complex seismic trace in a least-squares sense. (After Liu, 2006).

Theory: Implementation of the matching pursuit algorithm (continued)

Even if we attempted to approximate the seismic data using wavelets centered about all of the peaks of $e(t)$, the resulting residual $R(t)$ may still contain weaker seismic events of interest, implying an iterative solution to find them. Alternatively, isolated low amplitude events may represent noise, implying that we may wish to start with the highest amplitude event, estimate and subtract it, and iteratively repeat the process on the residual, giving rise to what is called a greedy matching pursuit algorithm (Mallat and Zhang, 1993). If we consider a thin bed tuning model where the top and bottom reflection events are nearly equal, resolvable, but interfere with each other, it is clear that the greedy matching pursuit will be biased. For this reason, Liu and Marfurt (2007) provide a parameter, $0 \le \beta \le 1$, that allows the interpreter to adjust how many events $k=1, 2, \ldots, K$ of the J envelope peaks are used in each iteration. Specifically,

$$k = \begin{cases} j \quad \text{if } e_k \ge \beta \underset{j}{MAX}\left(e_j\right) \\ null \text{ if } e_k < \beta \underset{j}{MAX}\left(e_j\right) \end{cases}, \tag{A-11}$$

where "null" indicates that that event is not used. The iteration continues until either an acceptable residual has been reached or if the convergence rate slows down to a level indicating numerical convergence.

To compensate for migration stretch, we simply replace the wavelets given by equation A-1 with the "non-stretched" wavelets f_k with compensated wavelets $c_k f_k$ described by equations 5 and 6 in the main part of this paper. We also apply the phase shift occurring in A_j to the real wavelet, w, rather than to the reflection coefficient, r_j:

$$u(t) = \mathrm{Re}\left[U(t)\right] = \mathrm{Re}\left[\sum_{j=1}^{J} r_j \exp\left(i\varphi_j\right) W_j(t - t_j,\, f_j) + N(\mathrm{t})\right] = \sum_{j=1}^{J} r_j w_j(t - t_j,\, f_j, \varphi_j) + n(\mathrm{t}) \tag{A-12}$$

Example

Figure 5a shows the input, unmuted CRP gather. Figure 5b shows the migration stretch compensated unmuted CRP gather. Figure 5c shows the data not modeled by the matching pursuit algorithm. Figure 5d shows the frequency compensation factor. The compensation factor increases with offset and decreases with depth, such that the far offset data of the shallower zone suffer from greater stretching. Note the higher resolution at the farther offsets at the Barnett Shale target at 1.1 s. The original unmuted CRP gather, and unmuted stretch compensated CRP gather were conditioned for simultaneous inversion.

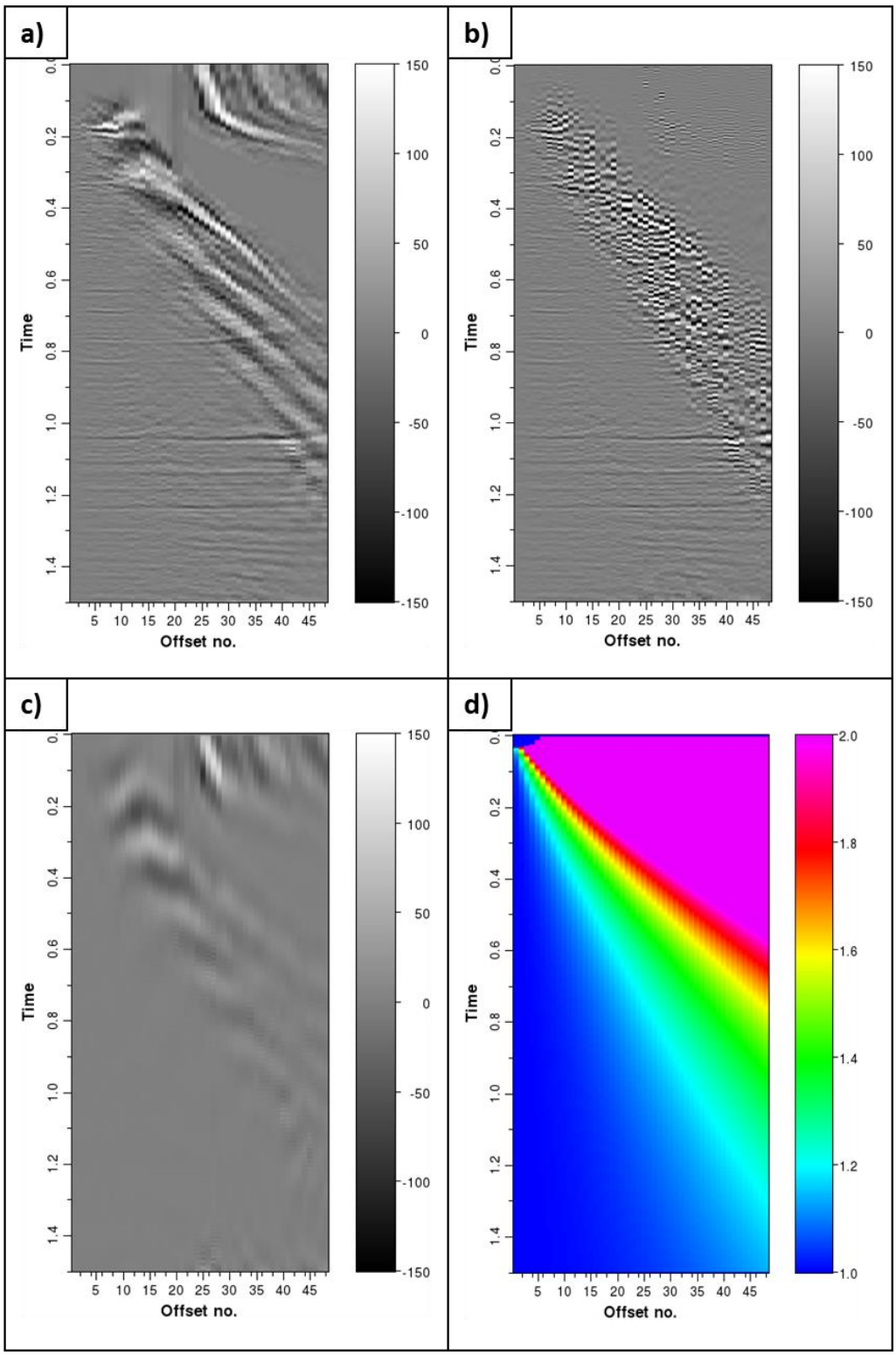

Figure 5. (a) The unmuted CRP gather of the data, (b) unmuted migration stretch compensated CRP gather, (c) unmodeled data and, (d) the frequency compensation factor. The farther the offset, the more frequency compensation factor.

Data Conditioning

In order to ascertain the value of the migration stretch, we applied the same suite of filters to the compensated and uncompensated gathers. First, we applied a seismic mute to remove high amplitude reverberations that overprint the shallow far-offset data. Then we applied parabolic Radon transform to discriminate between primaries and long period multiples. The gathers were transformed to velocity-stack domain, the low frequency noise is modelled and subsequently subtracted from the unmuted portion of the seismic gathers. Finally, we applied prestack structure-oriented filtering (Zhang et al., 2016) using a Lower Upper Median (LUM) to suppress noise crosscutting the reflectors of interest.

Figure 6a and 6b shows a conditioned CRP gather before and migration stretch compensation. Compensating for the migration stretch has considerably improved the resolution of the far offset data. Figure 7a and 7b shows that compensation for the migration stretch boosts high frequencies in the amplitude spectrum of the far angle stack (34^o-42^o) data. There is no compensation applied in the blue area of Figure 2d, such that the spectrum of the near offset data is unchanged.

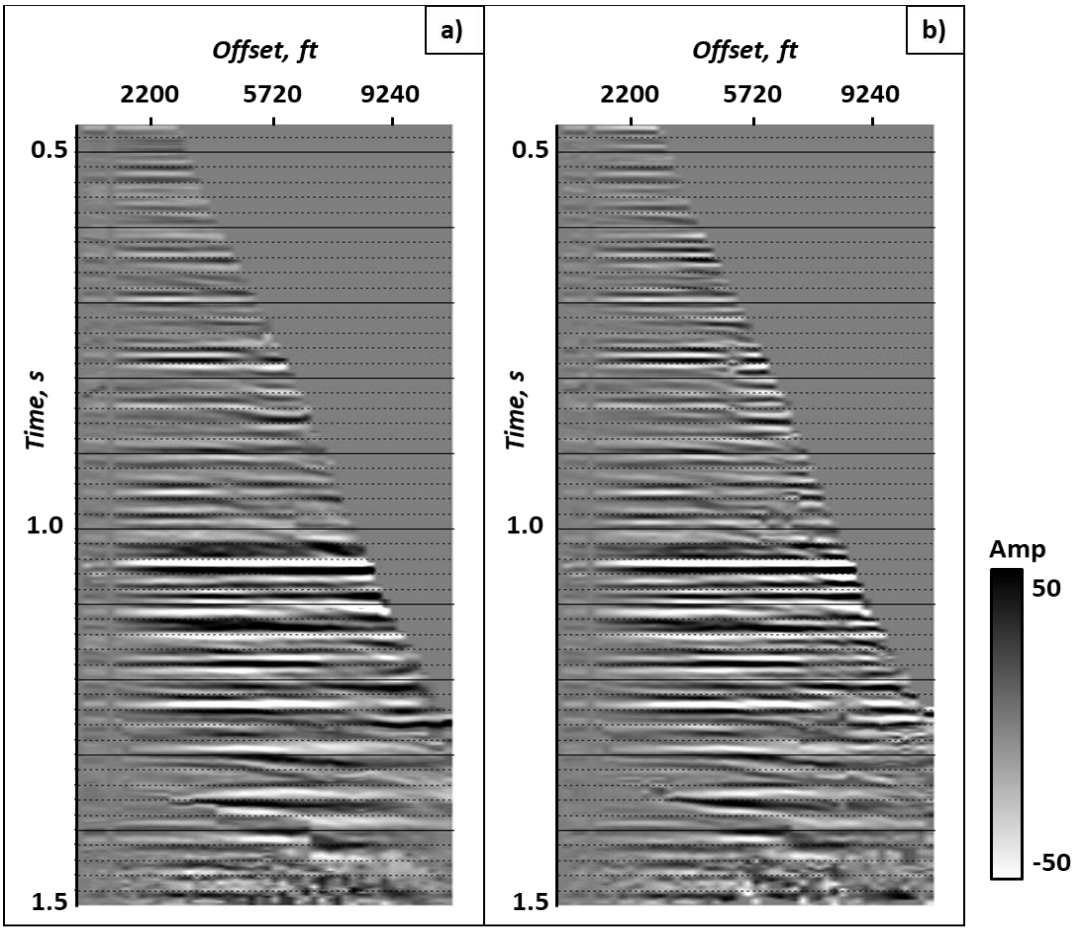

Figure 6. (a) Original CRP gather and (b) stretch compensated CRP after data conditioning. Both the data sets have been conditioned with same parameters. We observe an increase in resolution at far offset for stretch compensated data.

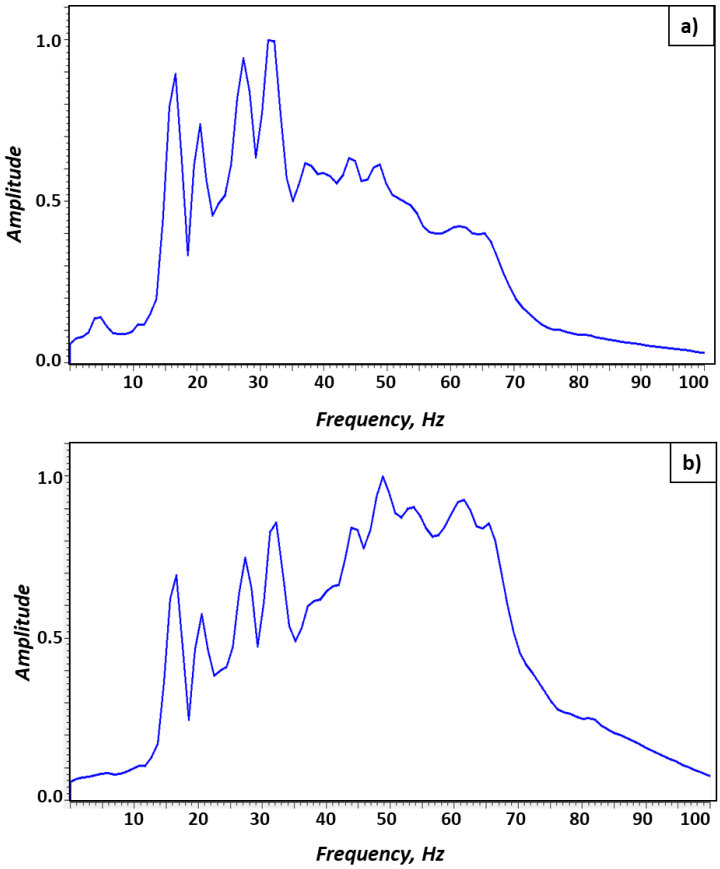

Figure 7. (a) Amplitude spectrum for far angle stack (34°-42°) for original CRP gather and (b) stretch compensated CRP gather. We observe a boost in the higher frequencies for the stretch compensated data.

Prestack simultaneous inversion

Figure 8 shows a cartoon of conventional "PP" seismic data acquisition. For a flat-layered geology and vertical incidence almost 100% of the near-offset reflected energy consists of PP reflections. Because the offset is small, the recorded seismic wavefield does not suffer from migration stretch. At farther offsets (Figure 8b), the PP reflected event now suffers from migration stretch. The amplitudes of these farther offset PP reflections are sensitive not only to the change in Z_P, but also to the change in Z_S and ρ Figure 9. The gradient of the change of the PP reflection amplitude with angle is sensitive to the Z_S contrast across the boundary while the curvature near the critical angle is sensitive to ρ. It is this sensitivity of the PP reflection events to changes in all three parameters that allows us to invert Z_S and density; unless we acquire multicomponent data, we do not measure the PS reflection events. While the PS reflection events will in general suffer from greater attenuation than the corresponding PP events, the lower resolution in Z_S and ρ compared to that of Z_P from PP reflected events is not due to attenuation but rather to the greater sensitivity of the Z_S inversion to the farther (stretched) offsets.

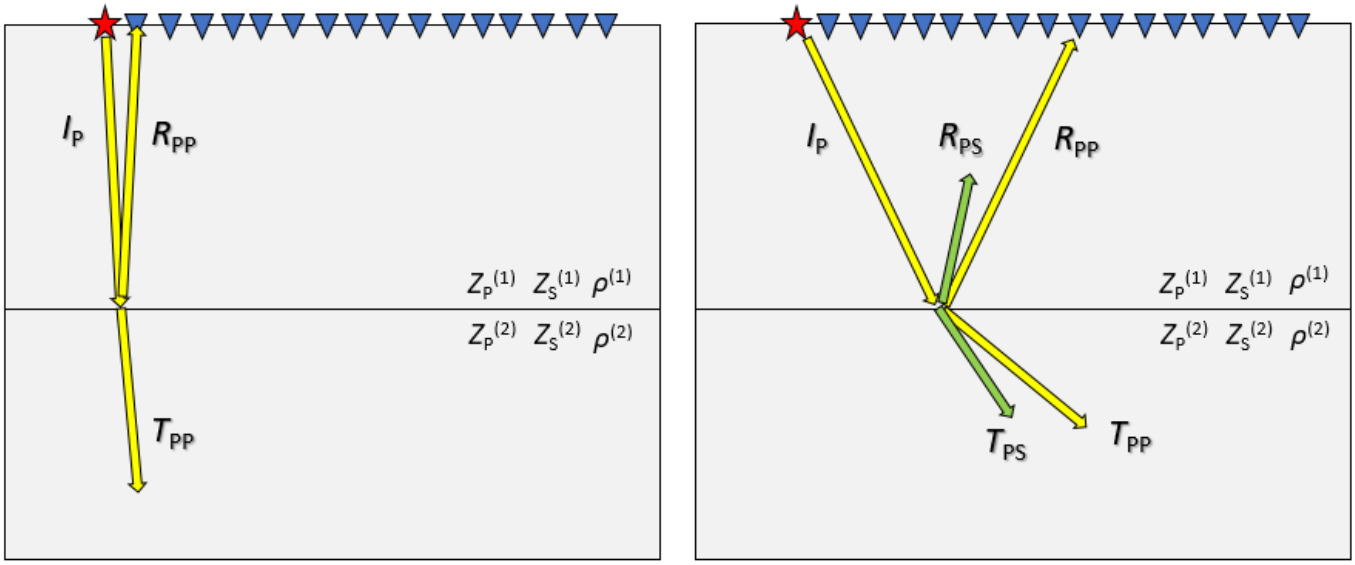

Figure 8. Cartoon showing the conventional "PP" seismic data acquisition using vertical geophones (on land) or hydrophones (at sea). (Left) For a flat-layered geology and vertical incidence almost 100% of the near-offset reflected energy consists of PP reflections. Because the offset is small, the recorded seismic wavefield does not suffer from migration stretch. (Right) At farther offsets, the PP reflected event now suffers from migration stretch. The amplitudes of these farther offset PP reflections are sensitive not only to the change in P-wave impedance ZP, but also to the change in S-wave impedances and density. It is this sensitivity of the PP reflection events to changes in all three parameters that allows us to invert S-impedance; unless we acquire multicomponent data, we do not measure the PS reflection events. While the PS reflection events will in general suffer from greater attenuation than the corresponding PP events, the lower resolution in S-wave impedance compared to that of P-wave impedance from PP reflected events is not due to attenuation but rather to the greater sensitivity of the S-impedance and density inversion to the farther offsets. Compensation for migration stretch corrects for this acquisition phenomenon and provides a means of computing P-wave and S-wave impedance volumes exhibiting comparable resolution.

Simultaneous inversion was carried out for original and stretch-compensated gathers to estimate Z_P, Z_S and ρ. The maximum usable incident angle of 42° at the Barnett Shale target allowed us to estimate ρ from inversion. Inversion of both data volumes was carried out exactly with the same parameters.

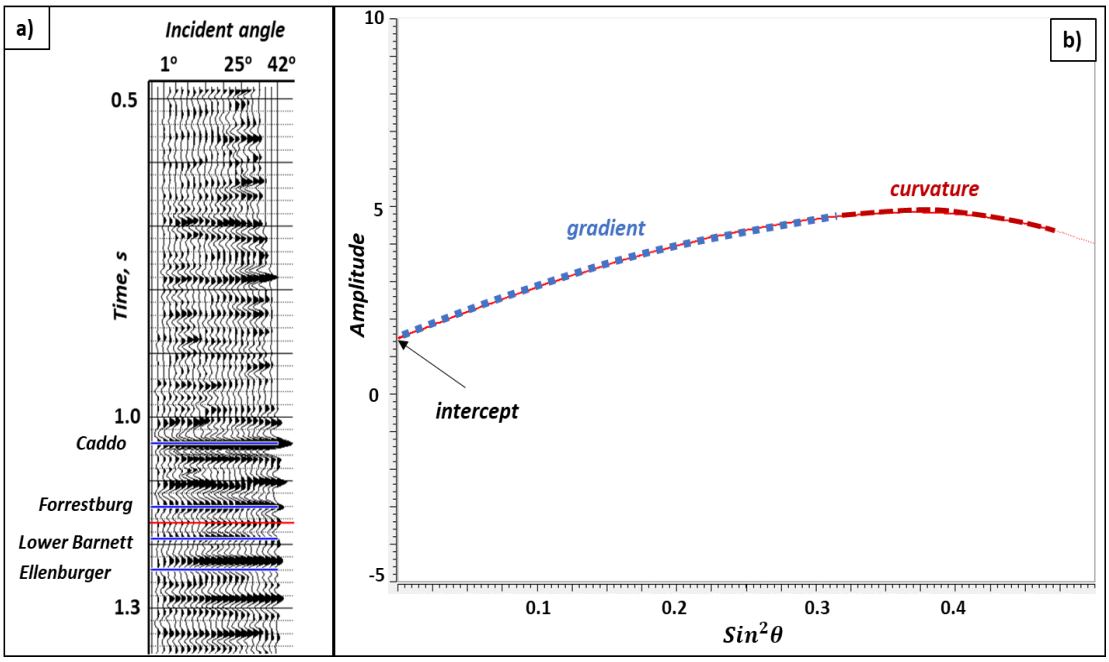

Figure 9. (a) A representative CRP gather with horizons in blue. (b) The AVO response of the event indicated by the red line in (a). The blue dashed line indicates the approximate AVO gradient. The red dashed line indicates the AVO curvature.

Figure 10a and 10b shows the Z_P estimated from simultaneous inversion of original prestack gather and migration stretch compensated gather respectively. A good match between the Z_{Plog} and $Z_{Pseismic}$ confirms the fidelity of the inversion. Because the near offsets that do not suffer from migration stretch are quite sensitive to changes in Z_P, there is little change in Z_P after stretch compensation (Figure 10).

Figure 11a-b shows Z_S and Figure 12a-b shows ρ estimated from simultaneous inversion of original prestack gathers and migration stretch compensated gathers respectively. A good match between the logs and inverted seismic volumes validates the fidelity in the inverted Z_S and ρ volumes. Compensation for migration stretch produces a significant improvement in resolution of the Z_S and ρ in the shallow section and reduced improvements deeper as predicted by Figure 5d.

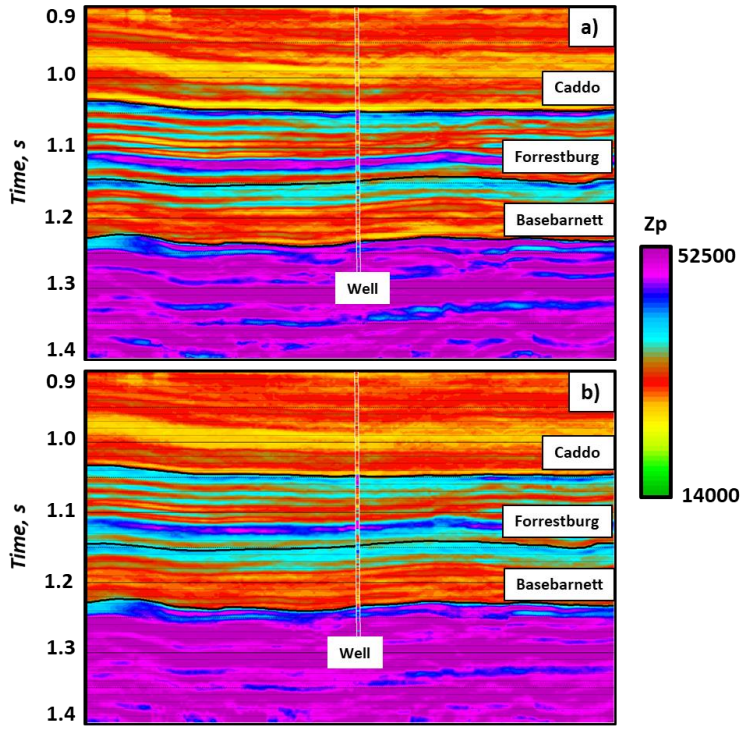

Figure 10. Z_P estimated from simultaneous inversion of a) original prestack gather and, b) migration stretch compensated prestack gather. We see insignificant improvement in resolution of Z_P from compensation of migration stretch

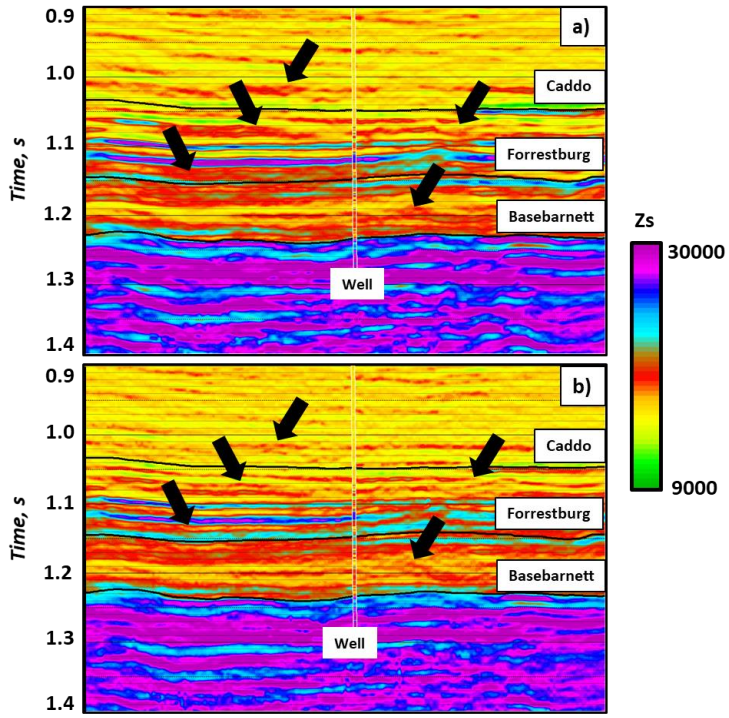

Figure 11. Z_S estimated from simultaneous inversion of (a) original prestack gather and, (b) migration stretch compensated prestack gather. The black arrows show areas of significant improvement in resolution of Z_S from compensation of migration stretch.

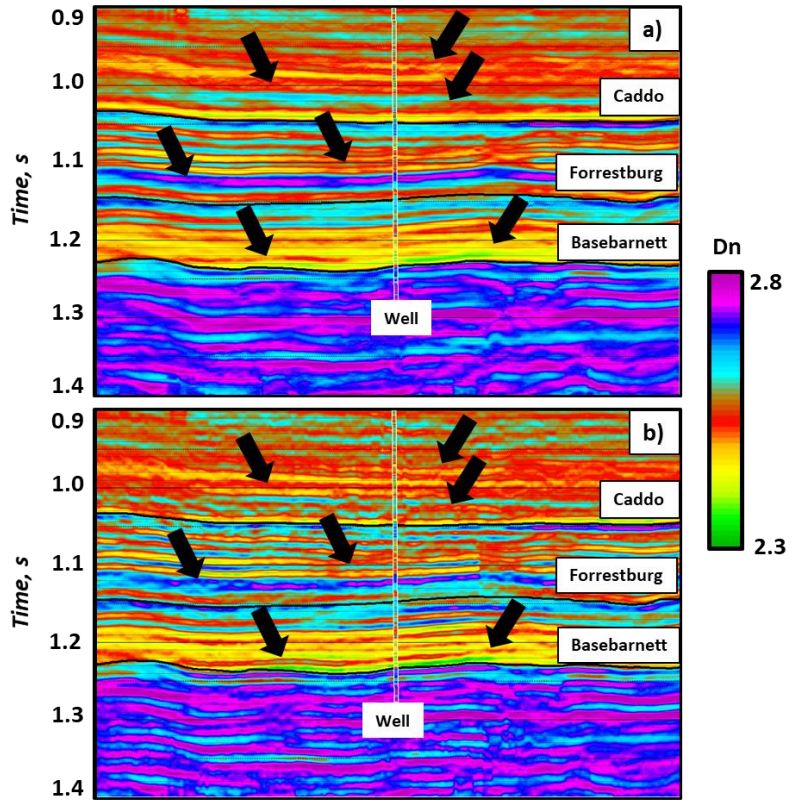

Figure 12. ρ estimated from simultaneous inversion of (a) original prestack gather and, (b) migration stretch compensated prestack gather. Black arrows indicate areas of significant improvement in resolution of ρ by compensating for migration stretch.

References

Liu, J., 2006, Spectral decomposition and its application in mapping stratigraphy and hydrocarbons: Ph. D. dissertation, University of Houston.

Liu, J., and K. J. Marfurt, 2007, Instantaneous spectral attributes to detect channels: Geophysics, **72**, P23-P31.

Mallat, S. and Z. Zhang, 1993, Matching pursuit with time-frequency dictionaries: IEEE transactions in signal processing, Dec. 1993.

Mutlu, O., and K. J. Marfurt, 2015, Improving seismic resolution of prestack time-migrated data: Interpretation, **3**, T245-T255.

Patel, S., F. O. Oyubanji, and K. J. Marfurt, 2019, Compensating for migration stretch to improve the resolution of S-impedance and density inversion: 89th Annual International Meeting of the SEG, Expanded Abstracts, xx-yy.

Zhang, B., K. Zhang, S. Guo, and K. J. Marfurt, 2013, Nonstretching NMO correction of prestack time-migrated gathers using a matching-pursuit algorithm: Geophysics, **78**, U9-U18.

Puryear, C. I., and J. P. Castagna, 2008, Layer thickness determination and stratigraphic interpretation using spectral inversion: Theory and application: Geophysics, **73**, R37–R48.